Article

Synthesis of Fine Micro-sized BaZrO Powders Based on a Decaoctahedron Shape by the Microwave-Assisted Hydrothermal Method

Ma#rio L. Moreira, Juan Andre#s, Jose# A. Varela, and Elson Longo

Cryst. Growth Des., **2009**, 9 (2), 833-839 • DOI: 10.1021/cg800433h • Publication Date (Web): 15 December 2008

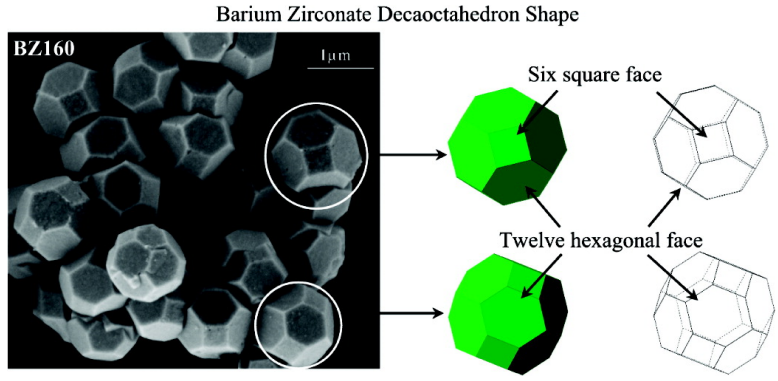

More About This Article

Additional resources and features associated with this article are available within the HTML version:

- Supporting Information
- Access to high resolution figures
- Links to articles and content related to this article
- Copyright permission to reproduce figures and/or text from this article

View the Full Text HTML

CRYSTAL GROWTH & DESIGN
2009
VOL. 9, NO. 2
833–839

Synthesis of Fine Micro-sized $BaZrO_3$ Powders Based on a Decaoctahedron Shape by the Microwave-Assisted Hydrothermal Method

Mário L. Moreira,[†] Juan Andrés,[‡] José A. Varela,[§] and Elson Longo*[,§]

LIEC, Departamento de Quimica, Universidade Federal de Sao Carlos, P.O. Box 676, 13565-905, Rod. Washington Luis, Km 235, Monjolinho, Sao Carlos - SP, Brazil, and LIEC, Departamento de Fisico-Quimica, Instituto de Quimica, Universidade Estadual Paulista, P.O. Box 355, 14801-907, R. Francisco Degni, s/n, Bairro Quitandinha, Araraquara - SP, Brazil

Received April 26, 2008; Revised Manuscript Received November 17, 2008

ABSTRACT: Micro-sized decaoctahedron $BaZrO_3$ powders were synthesized by means of a hydrothermal microwave method at 140 °C for 40 min. The X-ray diffraction, Raman, UV−visible, and inductively coupled plasma atomic emission (ICP-AES) spectroscopy, as well as measurements of photoluminescence (PL) emission, were used for monitoring the formation of a perovskite phase with random polycrystalline distortion in the structure. Two emissions at 477 and 526 nm were accompanied by increase in the gap values, indicating the existence of different emission mechanisms. A theoretical model derived from previous first principle calculations allow us to discuss the origin of the photoluminescence emission in $BaZrO_3$ powders which can be related to the local disorder in the network of both ZrO_6 octahedral and dodecahedral (BaO_{12}) hence forming the constituent polyhedron of $BaZrO_3$ system. Initial observations of a novel morphology of the $BaZrO_3$ perovskite crystal growth based on decaoctahedron shape is demonstrated and indirectly related to photoluminescence emissions.

1. Introduction

The controlled synthesis of desirable composition, size, shape, and crystal structure is of considerable interest because of its potential application to obtaining materials with wide technological applications. The continuing trend toward miniaturization requires techniques to produce materials with particle shape accuracy.[1] In particular; materials with ABO_3 perovskite-type structure have been the subject of a major focal point of interest in material science because they are of fundamental interest and technological importance. Recently, different studies have been performed on the barium zirconate, $BaZrO_3$ (BZ) ceramics, because of their promising properties[2] including a high dielectric permittivity of about 30 and a wide band gap with 5.3 eV.[3] BZ can be used as refractory material, as a substrate in the synthesis of superconductors, as high-temperature microwave dielectrics, as well as electro ceramic capacitors applicable in wireless communications.[4a−d] Because a refined control on the morphology of BZ powders is sought, a variety of processes have been employed. Many sizes and shapes have been obtained for BZ powders and other perovskite compounds, such as nanocubes[5] polyhedrons,[6a,b] nanowires,[4d,7a,b] and monodispersed particles,[8a,b] which have attracted vast attention because they exhibit unique optical, magnetic, and electronic properties which are not dependent only on the size but also on the shape of the particles.[7a]

Zirconates have been conventionally synthesized through solid-state reactions using zircon carbonates, oxides, and/or nitrate elements of group IIa to yield randomly shaped particles with broadly dispersed sizes. Solid state reactions are commonly performed at temperatures of up to 1300 °C[2] for the production of crucibles;[9] however, other synthetic procedures have been employed such as soft chemistry routes (polymeric precursor),[10] which allowed a systematic study of the evolution of the BZ phase, with diameter of 30−40 nm if they were synthesized by the sol−gel process[11] while an urea-induced precipitation process led to BZ nanoparticles with a diameter around 90 nm.[12] The high-energy dry grinding, laser ablation and spray pyrolysis usually requires long synthesis times using expensive and sophisticated equipments. Ultrafine powders of ZrO_2 have been converted into $MZrO_3$ (M = Ba, Sr, Ca) by both bath hydrothermal[13] and co-precipitation/calcinations[14] methods. The hydrothermal synthesis has been developed over the last decades to obtain nanometric BZ powders[15a−c] under fast and less expensive methods. Recently, microcrystalline (2−5 μm)[4c] and nanometric[15c] BZ powders were obtained using a hydrothermal synthesis process, working under supercritical conditions.

The conventional hydrothermal (CH) routes were normally conducted for several hours at temperatures higher than 200 °C.[16a,b] An interesting results was reported by Yun et al.[7a] who discussed the evolution of the morphology of barium zirconate morphology from truncated dodecahedral to a spherical shape by increasing the ethanol content in the water precursor solution. Moreover, these authors suggested a shape-dependent on photoluminescence (PL) emission with Eu-doped BZ microcrystals obtained at temperatures of the order of 130 °C for 12, 24, and 48 h,[7a] which requires the use of an airtight high-pressure vessel.

Recently, an alternative method using microwave heating has emerged in the field of powder preparation,[17a−i] with both expected and unexpected merits, for example, kinetic enhancement, low reaction temperature, time reduction, control of the overall particle size and aggregation process.[17a,h,18a,b] Rao et al. presented a summary of recent reports on the synthesis of inorganic materials using microwaves heating associated with hydrothermal conditions.[17a] In 1992, Komarmeni et al.[17b] introduced the hydrothermal microwave (HTMW) processing for synthesis of electro ceramic powders; this is a genuine low temperature and fast reacting method.[17c] A year later the same authors developed the synthesis of perovskite oxides for BZ based materials, which are usually found to have spherical

* To whom correspondence should be addressed. E-mail: elson@iq.unesp.br. Phone: +55 16 3361 5215. Fax: +55 16 3351 8350.
[†] Universidade Federal de Sao Carlos.
[‡] On leave from Departamento de Química Física y Analítica, Universitat Jaume I, 12071 Castelló, Spain.
[§] Universidade Estadual Paulista.

10.1021/cg800433h CCC: $40.75
Published on Web 12/15/2008

morphologies with a particle size range of about 0.1−0.5 μm. Recently, Maksimov et al.[19] prepared fine $BaZrO_3$ and $BaHfO_3$ powders by the HTMW process, and the results indicate that microwave processing during hydrothermal synthesis notably reduces the average particle size of the resulting powder and ensures a narrower particle size distribution in comparison with particles prepared by a CH process. Phani et al.[20] synthesized the nanocrystalline $ZnTiO_3$ perovskite thin films by the sol−gel process assisted by microwave irradiation. These authors have emphasized a dramatic change in the morphological properties of the films irradiated in microwave compared to the conventional treatment.

The HTMW process is a fast and very promising technique for ceramic materials. It offers significant advantages when compared with the CH method such as, reduced processing time, increased nucleation rate, homogeneous heating, hence, leading to the formation of smaller structures.[17a−i] Our group has significantly expanded the effort to demostrate that the HTMW method is one of the simplest, most versatile, and highly cost-effective approaches available to obtain crystalline, chemically pure, single-phase micro and/or nano scale materials at lower temperature and shorter reaction times with little residual impurities. The intrinsic scalability, flexibility, and facility of this method render it attractive for the fabrication of a wide range of perovskite based materials.[18a,21a,b] Godinho et al.[21b] observed the interesting fact that, under HTMW heating, the growth process of the gadolinium-doped cerium oxide system is faster than under hydrothermal electric heating. Thus, they postulated that electromagnetic microwave heating increases the effective collision rates during the process. The very simple, attractive, and novel procedure concentrates microwave radiation into the solution, thereby enhancing the structural and morphological properties.

The present work reports further progress on the synthesis of BZ powders using the HTMW method. In addition, the effects, as well as the merits, of microwave heating on the process and characteristics of the obtained BZ powders are reported. To the best of our knowledge, this is the first synthesis of microcrystalline BZ powders presenting a decaoctahedron shape. The corresponding structural properties and morphology were investigated and confirmed by means of various techniques: X-ray diffraction (XRD) including Rietveld refinements, UV−visible, ICP, and Raman spectroscopy. In addition, photoluminescence (PL) measurements at different times were performed at room temperature. This technique is an effective tool that provides important information on physical properties at molecular level defects and gap states.[22a,b]

2. Experimental Details

The BZ powders were synthesized using $ZrCl_4$ $5H_2O$ (99.9%, Aldrich), $BaCl_2$ $2H_2O$ (99%, Mallinckrodt), and KOH (P.a, Merck). The solutions were prepared as follows: in the first one, 0.05 mol of the $ZrCl_4$ $5H_2O$ was added to 125 mL of deionized water at room temperature under stirring until it turned into a transparent solution. Similarly, 0.05 mol of the $BaCl_2$ $2H_2O$ was dissolved in 125 mL of deionized water. The two precursor solutions were mixed, homogenized, and separated in five portions, and 50 mL of the KOH solution (6 M) were added in each solution under constant stirring to act as mineralizer, taking the co-precipitation of the Zr and Ba hydroxides to form the reaction mixture.

The reaction mixture was loaded in a 110 mL Teflon autoclave reaching 90% its volume, hence providing maximum pressure efficiency,[23] which was sealed and placed in the microwave-hydrothermal system using 2.45 GHz microwave radiation with maximum power of 800 W.[24] The reaction mixture was heated in less than 1 min to 140 °C and kept at this temperature for $BaZrO_3$-Xmin, where X = 10 (BZ10), 20 (BZ20), 40 (BZ40), 80 (BZ80), and 160 min (BZ160), without agitation and under constant pressure of 2.5 bar. After the reaction, the autoclave was naturally cooled to room temperature. Next, the solid product was washed with deionized water several times until neutral pH, and then, dried overnight at 80 °C.

3. Characterizations

The samples were characterized by XRD (Rigaku DMax 2500PC) using Cu Kα (λ = 1.5406 Å) radiation. The data were collected from 10° to 120° in the 2θ range with 0.5° divergence slit, 0.3 mm receiving slit, in fixed-time mode with 0.02° step size and Is/point. Crystal structures were identified and refined by the Rietveld method[25] using the GSAS[26] software. This software is specially designed to refine simultaneously both the structural and the microstructural parameters through a least-squares method. The peak profile function was modeled using the convolution of the Thompson-Cox-Hastings pseudo-Voigt (pV-TCH) with the asymmetry function described by Finger et al.[27] The background of each pattern was fitted by a polynomial function.

An inductively coupled plasma atomic emission spectrometer ICP-AES Simultaneous CCD - VISTA - MPX (Varian, Mulgrave, Australia) with radial configuration was used for chemical analyses. The operating conditions are the following: 40 Mhz frequency, 100 kW power, in a radial plasma view configuration. Background signal correction was carried out by the instruments operating software. Microstructural and morphological characterization were performed by field emission scanning electron microscopy (FE-SEM, Zeiss Supra 35).

Raman spectra were recorded on a RFS/100/S Bruker Fourier transform (FT-Raman) spectrometer, with Nd:YAG laser excitation light at 1064 nm in a spectral resolution of 4 cm^{-1}. UV−vis absorption of the optical absorbance for $BaZrO_3$ decaoctahedrons was taken using Varian Cary 5G equipment. Photoluminescence (PL) spectra were collected with a Thermal Jarrel-Ash Monospec 27 monochromator and a Hamamatsu R446 photomultiplier. The 350.7 nm (3.52 eV) exciting wavelength of a krypton ion laser (Coherent Innova) was used, with output power of the laser kept at 200 mW. All measurements were taken at room temperature.

4. Results and Discussion

XRD patterns of the samples treated from 10 to 160 min, corresponding until BZ10 to the BZ160 samples, respectively, are presented in Figure 1, which also reports the BZ unitary cell with the main diffraction plane (110), indicating that this diffraction is related to the periodic ordination of dodecahedral (BaO_{12}) and octahedral (ZrO_6) sites. One can observe a pattern of a crystalline material composed by BZ cubic structure from JCPDS card No. 06-0399 with *Pm*3*m* space group and a weak amount of orthorhombic witherite $BaCO_3$ phase from JCPDS card No. 05-0378 with the *Pmcn* space group especially noticed for the BZ10 sample. The low crystallinity and the small amount of amorphous material observed in the XRD of the BZ10 sample indicates that the crystallization process remain incomplete up to 10 min. After 20 min, the cubic BZ phase can be clearly identified in Figure 1 by the aforementioned JCPDS card. However, for 40 min (BZ40) during the HTMW process, it renders the existence of intense diffractions peaks marked as BZ phase together with a very low intensity peak at 2θ = 26° associated with the most intense diffraction of the witherite phase. For samples BZ80 and BZ160, Figure 1 illustrates the high crystalline BZ powders, without background and with smallest amount of $BaCO_3$ phase (<0.6%).

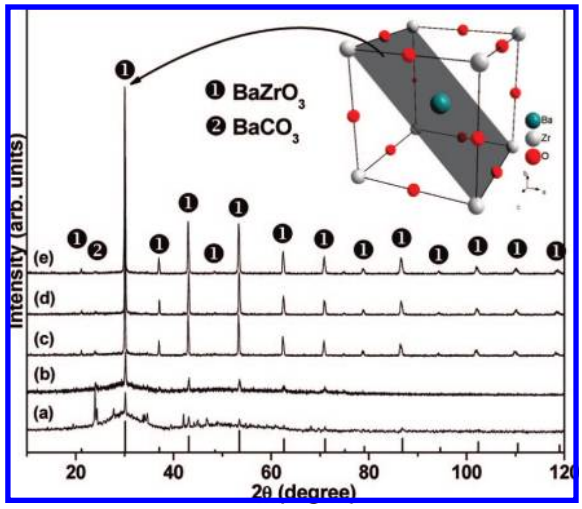

Figure 1. XRD of $BaZrO_3$ powders obtained for (a) 10 (BZ10), (b) 20 (BZ20), (c) 40 (BZ40), (d) 80 (BZ80), and (e) 160 (BZ160) at 140 °C by the HTMW method. Also shown is the BZ unitary cell with the main diffraction plane (110).

Table 1. Rietveld Parameters of $BaZrO_3$ Powders According to HTMW Time Treatment

	parameters					
sample	$a = b = c$ (Å)	χ^2	R-Bragg BZ (%)	R-Bragg $BaCO_3$ (%)	$BaCO_3$ (%)	R_{wp} (%)
BZ40	4.211584	2.1	2.0	8.1	1.6	6.33
BZ80	4.208129	1.7	1.5	6.3	1.2	5.48
BZ160	4.206291	1.9	1.3	11.5	0.6	6.0

Rietveld refinements were recorded for samples BZ40, BZ80, and BZ160 to obtain a deeper insight into the evolution of the barium zirconate phase. The BZ10 and BZ20 samples were not refined, as they do not correspond to the barium zirconate phase as indicated by the Raman, X-ray, and low Ba/Zr ratio obtained from ICP-AES measurements. The refinement continues until convergence is reached with the value of the quality factor, χ^2, approaching 1, which confirms the goodness of the refinement.[28] In this case, the BZ160 sample reports the more ordered structure among the samples, due to great $\chi^2 = 1.9$ and $R_{wp} = 6\%$ parameter values besides the smallest value for R-Bragg. Furthermore, the refined lattice parameters reported in the Table 1 for BZ160 are the closest to the JCPDS card No. 06-0399, ($a = b = c = 4.18$ Å). Another important factor is related to the 1.6% amount of barium carbonate phase for the BZ40 sample and the 0.6% for the BZ160 sample. The increasing values of R-Bragg for the BZ160 sample occur because there is only one indexed peak for the $BaCO_3$ phase, undermining the adjustment of the deleterious phase as depicted in the Figure 2, which represent a typical Rietveld refinement analysis output for assessing the quality of fitting.

Figure 3 illustrates all the typically Raman modes of the $BaCO_3$ phase.[29] The wide and weak vibrational modes at 381 and 544 cm^{-1} are related to the *m*-zirconia phase. However, the others Raman modes of the *m*-zirconia were not observed because of the superposition of the vibrational modes of the $BaCO_3$.[30a−e] Thus, after 10 min of synthesis, the orthorhombic barium carbonate and monoclinic ZrO_2 phase were favored instead of the cubic BZ phase. An analysis of the micrographies presented in Figure 4a point out that this sample is associated to nearly spherical or equi-axed agglomerates generated by the smaller particles self-assembly.

The Raman spectrum of BZ20 sample depicted in Figure 3 supplies the same information observed for the BZ10 sample.

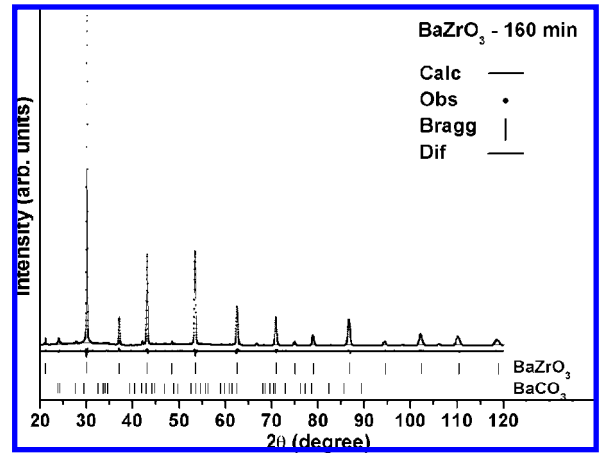

Figure 2. Rietveld refinement of the $BaZrO_3$ powders synthesized by the HTMW method at 140° for 160 min.

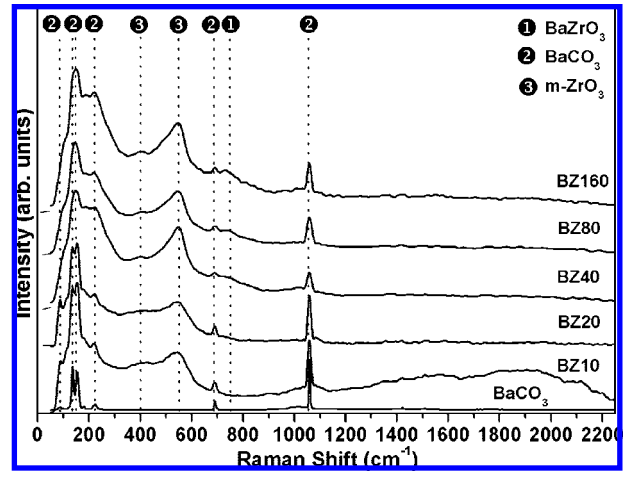

Figure 3. Raman spectra of the $BaZrO_3$ powders obtained from 10 up to 160 min at 140 °C.

The low crystallinity, evidenced by XRD, indicates that the crystallization process remains incomplete up to 20 min, while in Figure 4b the morphologies start turning into a multifaceted shape; however, they are still badly defined and in the same manner as described for the BZ10 sample. For the BZ40 sample the monoclinic zircon phase is described as a natural reaction in aqueous medium; however, Raman characteristic modes of *m*-ZrO_2 could not be all observed.[31,32] On the other hand, after 40 min of the process, the BZ phase becomes stable and the decaoctahedron shapes become evident (Figure 4c). The decaoctahedron shape exhibits 18 faces, 6 square and 12 hexagonal faces. However, a discharge superficial porosity can be observed (inset Figure 4c), in addition to badly defined face contours.

The micrographs in Figure 4d,e show highly defined decaoctahedron shapes, with low face porosity together with the well defined face contour. Thus, the sample processed for 160 min (BZ160) presents a more regular morphology. Local and dynamic symmetry of the Raman spectra for samples BZ40, BZ80, and BZ160 report a new weak mode at 758 cm^{-1}. This mode can be associated to the presence of a slightly distorted ZrO_6 octahedron.[33] Therefore, this fact points out that after 40 min of synthesis, the disordered cubic barium zirconate phase became more favored than the barium and zirconium individual phases. Lee et al.[34] reported that OH^- ions are important in the nucleation of $BaTiO_3$ powders under hydrothermal conditions, and these ions also seem to act as catalysts to accelerate the

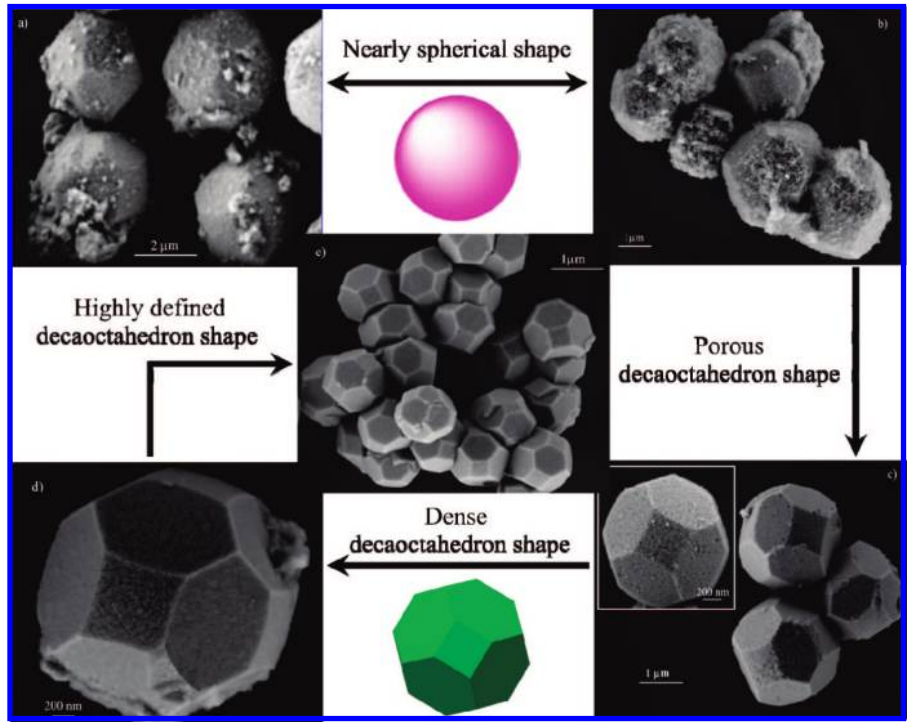

Figure 4. FE-SEM image of nearly spherical $BaZrO_3$ powders obtained for (a) 10 and (b) 20 min, and of decaoctahedral $BaZrO_3$ powders obtained for (c) 40, (d) 80, and (e) 160 min.

transition of Ba-OH bonds to $BaTiO_3$ crystals. In a similar way, the KOH concentration in the sheath acts on the formation of the BZ powders. This non-thermal effect yields an increase of the diffusion rate and a decrease of the activation energy by polarization molecules.[24]

On the other hand, the viscosity of the water decreases with increasing temperature. Under hydrothermal conditions at 500 °C and 10 bar, the water has only 10% of its viscosity under ambient conditions. Even under milder conditions, the viscosity is still low,[35] and thus it may be conceived that the mobility of dissolved ions and molecules is higher under hydrothermal conditions than at ambient pressure and temperature, taking into account the increase of the effective collision rate in the solution that occurs when particles collide, hence producing irreversibly oriented attachments during the HTMW processing.[36a] Besides, the use of the microwaves energy acts directly on the rotational barriers of the water employing uniform ratings[36a,b] and are enhanced by one or two orders of magnitude of the crystallization kinetic behavior[17b,c] because of a direct interaction of radiation with matter. These conditions offer a favorable medium for the formation of barium zirconate oxide at low temperatures and short annealing times.

The agglomeration process can be related to the van der Waals forces; then, to reduce surface energy, the primary particles have a basic tendency to form self-assembled agglomerations, originating nearly spherical or equi-axed agglomerates with a minimum surface to volume ratio; hence, minimum surface free energy can be achieved.[37] After this process is observed for samples BZ10 and BZ20, the agglomerated particles start the growth of multifaceted shapes to form a stable decaoctahedron shape for the BZ40, BZ80, and BZ160 samples as recorded in Figure 4.

XRD, Raman, and ICP-AE spectroscopy recordings are used to carry out an analysis of the crystal morphology evolution along the synthetic process. The results seem to indicate for samples BZ10 and BZ20 that the dissolution of the barium carbonate and *m*-zirconia takes place, supplying the initial formation of the barium zirconate phase. After 40 min of processing, the BZ phase can indeed be signaled as preferential and sitable crystalline cubic phase with well defined decaoctahedron shapes (Figure 4c−e), besides a better Ba/Zr ratio as follows.

Table 2. Nominal and Experimental Compositions of $BaZrO_3$

	composition, in % molar fraction	
	nominal	analyzed[a]
ceramic denomination	*x* Ba/Zr	*x* Ba/Zr
BZ10	1	0.97 ± 0.006
BZ20	1	0.98 ± 0.002
BZ40	1	0.99 ± 0.003
BZ80	1	0.99 ± 0.003
BZ160	1	0.99 ± 0.002

[a] $n = 5$ (n = measures).

ICP-AES spectroscopy was used to determine the Ba/Zr ratio, as well as the purity degree of the samples. To estimate the accuracy of the determinations in the BZ solutions with lower salt concentrations, two series of 1:10 and 1:100 dilutions were prepared from the original digested samples. The dissolution procedure was carried out using 10 mL of HCl (37% m/m) and 3 mL of HNO_3 (68% m/m) in closed vessels at room temperature for 2 h. Analytical blanks were prepared following the same acid digestion procedure. Table 2 shows the nominal compositions of the powders, and the concentration of impurities (Ca + Sr + Mg) lesser than 1 ppm is achieved.

The performance of the material (optical, electric, and structural properties) is not only sensitive to pore sizes (1 to 100 nm) but also to access to the pore network that depends on particle size (1 to 100 mm) and morphology;[38] then, dense particles are desirable specially for electrical applications. The decaoctahedron shape is an important factor regarding the degree of disorder that leads to an incomplete circumference (the decaoctahedron circumference is less than 360°) hence causing

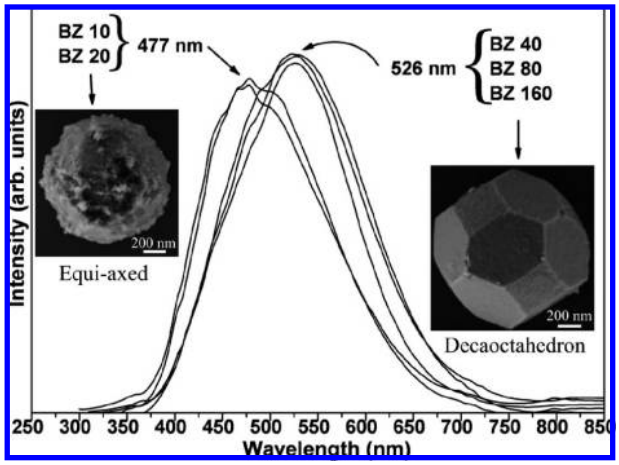

Figure 5. Photoluminescence spectra of equi-axed and decaoctahedrons $BaZrO_3$ samples.

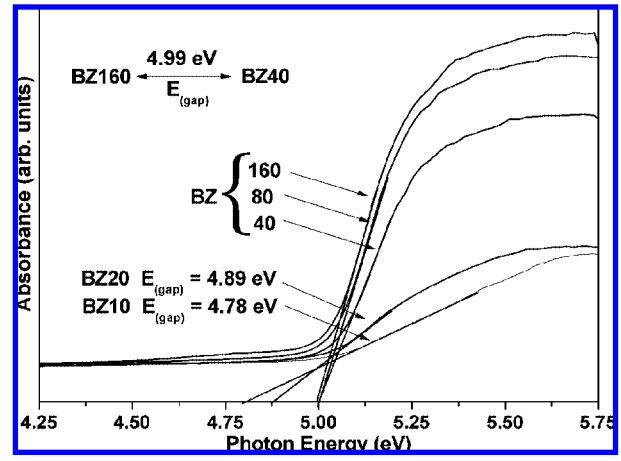

Figure 6. UV−visible gap dependence of $BaZrO_3$ phase and growth of the particles.

network tensions similar to that shown for the decahedron by Wang et al.[39] subsequently, tensions will surely be induced in the particles.

Meng et al.[40] proposed that the PL emission band increases the intensity with decrease of the grain size, which is closely correlated with interfaces of nanocrystallites (<100 nm) and d-surface states in the forbidden gap by the distortion of the TiO_6 octahedra. In our case, (Figure 5) the samples present a micro-sized decaoctahedron shapes; therefore, the PL emissions cannot be attributed only to the size of the crystals (nanosized). Furthermore, Cavalcante et al.[10] developed a consistent discussion regarding the evolution of the structural order of barium zirconate, based on the existence of zircon complex clusters in the BZ matrix, such as:

$$[ZrO_6]^x + [ZrO_5V_0^x] \rightarrow [ZrO_6]' + [ZrO_5V_0^{\bullet}]$$

$$[ZrO_6]^x + [ZrO_5V_0^{\bullet}] \rightarrow [ZrO_6]' + [ZrO_5V_0^{\bullet\bullet}]$$

$$[ZrO_5V_0^{\bullet}] + \frac{1}{2}O_2 \rightarrow [ZrO_6]$$

When $[ZrO_6]^x \gg [ZrO_5V^{\bullet}_0]$ and/or $[ZrO_5V^{\bullet}_0] = 0$, the PL emission is quickly reduced. For these octahedral complex clusters the authors attributed the formation of localized levels within the band gap, for disordered samples thermally treated at temperatures between 350 and 600 °C. Therefore, no PL emission was observed for samples heat treated at 700 °C by 2 h in a conventional furnace, which was described as the more ordered structure (structurally sample $[ZrO_5V^{\bullet}_0] = 0$). In the other samples heat treated at lower temperatures (<700 °C) the existence of a significant relationship between $[ZrO_6]^x$ and $[ZrO_5V^{\bullet}_0]$ clusters allowed the polarization system.

Leite et al.[41a] reports the typical PL emission of disordered barium zirconate powders at room temperature around 585 nm, and Cavalcante et al. reports the PL emission for the same material at around 540 nm,[10] using the same wavelength excitation. Therefore, the PL emission of BZ40, BZ80, and BZ160 presents more ordered structures than observed by them, because of a large blue-shift emission centered at 526 nm (Figure 5). However, a certain disorder degree must persist in the ZrO_6 octahedral site which allows the formation of the intermediate levels within the barium zirconate band gap.[41a,b]

Thus, the PL emission can be attributed to the freezing of structural defects inside the zirconium octahedrons, which are related to the use of the microwave energy acting directly on the rotational barriers of the water providing a high heating rate (around 120°/min) and increase the self-assembled pressure, hence forcing the fast formation of distorted BZ (quasi-crystalline) powders. With the increase of the thermal treatment time, it can be perceived from the Rietveld refinement data that the unitary cell tends to relax the structural tensions approaching the system with more ordered structure.

The structural properties associated with both distorted octahedral (ZrO_6) and dodecahedral (BaO_{12}) clusters forming the constituent polyhedrons of $BaZrO_3$ system are crucial for the PL property of this system. This seems to be general for the perovskite-based materials. The slight distortions on the ZrO_6 octahedron are corroborated by Raman spectra due to the existence of the weak signal at 758 cm^{-1},[33] which are responsible for the polarization of the structure, just as proposed by Meng et al.[10,41b,42] On the other hand, non-substantial distortions were observed on the dodecahedral BaO_{12} sites. Besides, the PL emission at 477 nm corresponds to a non-uniform structure of the BZ phase, associated with *m*-zirconia structure as previously discussed in the Rietveld refinements section.[36a,41b]

In our proposed model, the wide-band model [22b,42] for PL emission of the barium zirconate samples, the most important events occur before excitation, that is, before the arrival of the photon. The short and intermediate range structural defects generate localized states within the band gap and a non-homogeneous charge distribution in the cell thereby allowing electrons to become trapped. The localized levels are energetically distributed, so that various energies are able to excite the trapped electrons[22b] and the recombination of the excited trapped electrons gives a PL emission.

The same type of PL emission behavior can be observed in the UV−visible measurements in Figure 6, which reveal a typical absorbance for crystalline materials in the high energy region and two other absorbancies in the low energy region, suggesting large non-uniform distribution states within the band gap. The optical energy band gap is related to the absorbance and the photon energy by the following equation according to Wood and Tauc:

$$h\upsilon\alpha \propto (h\upsilon - E_g^{opt})^2 \qquad (2)$$

where α is the absorbance, h is the Planck constant, υ is the frequency, and (E_g^{opt}) is the optical band gap.[43]

The equi-axed shape for samples BZ10 and BZ20 results in optical gap values of 4.78 and 4.89 eV, respectively, which are smaller than the gap of highly structural BZ powders (5.3 eV).[3]

When the structures of BZ becomes predominant in the samples BZ40, BZ80, and BZ160, a well defined decaoctahedron shape is observed; then, the band gap values tend to the values of structurally ordered barium zirconate powders (5.3 eV)[3] and higher than for more ordered samples obtained by Cavalcante et al.[10] On the other hand, structural distortions at octahedral sites provoke the PL emission shift to the blue region in the visible spectra and actually present a distorted structure. The band gap energy is much higher than the excitation energy used to record of PL spectra (3.54 eV). This fact seems to indicate the probability that certain localized levels exist within the band gap because the direct electron transition between the valence band and the conduction band is not allowed.[36a]

The exponential optical absorption edge and hence the optical band gap are controlled by the structural order−disorder degree on the BZ lattice. The decrease of the band gap can be directly associated with the increase of defects in the BZ lattice (octahedral distortion), which raises the intermediary levels within the band gap region, supplying a fundamental condition for the existence of polarizations and PL emission. Thus, the reduction to 4.99 eV of the band gap (for more ordered HTMW samples) can be related to the distortions on the ZrO_6 octahedral clusters in a cubic barium zirconate phase,[41a−c] evidenced by the Raman spectra as a weak signal at 758 cm^{-1}.[33]

5. Conclusion

In summary, micro-sized decaoctahedron shaped BZ powders were successfully synthesized using the HTMW method. This technique offers clean, low cost-effective, energy efficient, quite faster, and convenient method of heating, which results in higher yields and shorter reaction times in comparison with CH, complex polymerization, and solid state reactions because of the increase of the effective collision rate and the consequent favorable growth of BZ crystals by successive attachments. We believe that this mechanism is able to promote the formation of defects and/or distortions on the BZ polyhedrons. According to XRD, Raman spectra, UV−visible absorbancies, ICP-AES spectroscopy, and FE-SEM microscopy, the powders after 40 min in the HTMW system present a predominance of the barium zirconate phase that composes novel micro-sized decaoctahedron shapes. The presence of two PL emissions centered at 477 and 526 nm, as well as the time evolution of the band gap energies, seems to indicate the existence of two different emission mechanism for the processed material at different times. A theoretical model derived from previous first principle calculations allows us to discuss the origin of PL emission in $BaZrO_3$ powders. This behavior can indeed be assigned to the local disorder in the network of both ZrO_6 octahedral and dodecahedral (BaO_{12}), hence forming the constituent polyhedron of the BZ system, owing to the fact that if one of the polyhedrons is distorted it should have consequent distortions on the other, as they share the same crystalline net. In this work, we have shown that by means of the HTMW synthetic method, reliable size, shape, and composition control can be achieved to obtain micro-sized decaoctahedron BZ powders, opening the door for advanced materials as promising candidates for future catalysis applications.

Acknowledgment. The authors acknowledge the support of the Brazilian agencies CAPES, CNPq, and FAPESP/CEPID 98/14324-8. J.A. acknowledges by research funds provided by the *Ministerio de Educación y Cultura* of the Spanish Government to carry out a research stay. We thank Diogo Volanti, Rorivaldo Camargo, and Madalena Tursi for their technical contributions.

References

(1) Mao, Y.; Wong, S. S. *Adv. Mater.* **2005**, *17*, 2194–2199.
(2) Zhou, H.; Mao, Y.; Wong, S. S. *Chem. Mater.* **2007**, *19*, 5238–5249.
(3) Robertson, J. *J. Vac. Sci. Technol. B.* **2000**, *18*, 1785–1791.
(4) (a) Erb, A.; Traulsen, T.; Muller-Vogt, G. *J. Cryst. Growth* **1994**, *137*, 487–492. (b) Macmanus-Driscoll, J. L.; Foltyn, S. R.; Jia, Q. X.; Wang, H.; Serquis, A.; Civale, L.; Maiorov, B.; Hawley, M. E.; Maley, M. P.; Peterson, D. E. *Nat. Mater.* **2003**, *3*, 439–443. (c) Kolen'ko, Y. V.; Burukhin, A. A.; Churagulov, B. R.; Oleinikov, N. N.; Vanetsev, A. S. *Inorg. Mater.* **2002**, *38*, 252–255. (d) Bennett, J. W.; Grinberg, L.; Andrew, M. R. *Phy. Rev. B* **2006**, *73* 180102(R), 1–4.
(5) Mao, Y. B.; Banerjee, S.; Wong, S. S. *J. Am. Chem. Soc.* **2003**, *125*, 15718–1519.
(6) (a) Dias, A.; Ciminelli, V. S. T. *Chem. Mater.* **2003**, *15*, 1344–1349. (b) Lu, Z.; Tang, Y.; Chen, L.; Yadong, L. *J. Cryst. Growth* **2004**, *266*, 539–544.
(7) (a) Urban, J. J.; Spanier, J. R.; Ouyang, L.; Yun, W. S.; Park, H. *Adv. Mater.* **2003**, *15*, 423–426. (b) Yun, W. S.; Urban, J. J.; Gu, Q.; Park, H. *Nano Lett.* **2002**, *2*, 447–450.
(8) (a) OBrien, S.; Bras, L.; Murray, C. B. *J. Am. Chem. Soc.* **2001**, *123*, 12085–12086. (b) Liu, C.; Zou, B. S.; Rondinone, A. J.; Zhang, Z. J. *J. Am. Chem. Soc.* **2001**, *123*, 4344–4345.
(9) Kirby, N. M.; Trang, A.; Riessen, V. A.; Buckley, C. E.; Wittorff, V. W.; Cooper, J. R.; Panagopoulos, C. *Supercond. Sci. Technol.* **2005**, *18*, 648–657.
(10) Cavalcante, L. S.; Longo, V. M.; Zampieri, M.; Espinosa, J. W. M.; Pizani, P. S.; Sambrano, J. R.; Varela, J. A.; Longo, E.; Simões, M. L.; Paskocimas, C. A. *J. Appl. Phy.* **2008**, *103* (063527), 1–8.
(11) Veith, M.; Mathur, M.; Lecerf, N.; Huch, V.; Decker, T.; Beck, H. P.; Eiser, W.; Haberkorn, R. *J. Sol-Gel Sci. Technol.* **2000**, *17*, 145–158.
(12) Boschini, F.; Robertz, B.; Rulmont, A.; Cloots, R. *J. Eur. Ceram. Soc.* **2003**, *23*, 3035–3042.
(13) Kutty, T. R. N.; Vivekanandan, R.; Philip, S. *J. Mater. Sci.* **1990**, *25* (8), 3649–3658.
(14) Brzezinska-Miecznik, J.; Haberko, K.; Bucko, M. M. *Mater. Lett.* **2002**, *56* (3), 273–278.
(15) (a) Gopalakrishnan, J. *Chem. Mater.* **1995**, *7*, 1265–1275. (b) Hirano, M. *Recent Res. Dev. Mater. Sci.* **2002**, *3*, 563–577. (c) Aimable, A.; Xin, B.; Millot, N.; Aymes, D. *J. Solid State Chem.* **2008**, *181*, 183–189.
(16) (a) Fuenzalida, V. M.; Pilleux, M. E. *J. Mater. Res.* **1995**, *10*, 2749–2754. (b) Pilleux, M. E.; Grahmann, C. R.; Fuenzalida, V. M. *Appl. Surf. Sci.* **1993**, *65*, 283–288.
(17) (a) Rao, K. J.; Vaidhyanathan, B.; Ganguli, M.; Ramakrishnan, P. A. *Chem. Mater.* **1999**, *11*, 882–895. (b) Komarneni, S.; Roy, R.; Li, Q. *Mater. Res. Bull.* **1992**, *27*, 1393–1405. (c) Komarneni, S.; Li, Q.; Stefansson, K. M.; Roy, R. *J. Mater. Res.* **1993**, *8*, 3176–3183. (d) Abothu, I. R.; Liu, S. F.; Komarneni, S.; Li, Q. H. *Mater. Res. Bull.* **1999**, *34*, 1411–1419. (e) Bondioli, F.; Ferrari, A. M.; Leonelli, C.; Siligardi, C.; Pellacani, G. C. *J. Am. Ceram. Soc.* **2001**, *84*, 2728–2730. (f) Corradi, A. B.; Bondioli, F.; Focher, B.; Ferrari, A. M.; Grippo, C.; Mariani, E.; Villa, C. *J. Am. Ceram. Soc.* **2005**, *88*, 2639–2641. (g) Sun, W.; Liu, W. Li. *J. Powder Technol.* **2006**, *166*, 55–59. (h) Clark, D. E.; Sutton, W. H. *Annu. Rev. Mater. Sci.* **1996**, *26*, 299–331. (i) Booske, J. H.; Cooper, R. F.; Freeman, S. A. *Mat. Res. Innovat.* **1997**, *1*, 77–84.
(18) (a) Volanti, D. P.; Keyson, D.; Cavalcante, L. S.; Simões, A. Z.; Joya, M. R.; Longo, E.; Varela, J. A.; Pizani, P. S.; Souza, A. G. *J. Alloys Compd.* **2008**, *459*, 537–542. (b) Shi, S.; Hwang, J. Y. *J. Miner. Mater. Charact. Eng.* **2003**, *2*, 101–110.
(19) Maksimov, V. D.; Meskin, P. E.; Churagulov, B. R. *Inorg. Mater.* **2007**, *47*, 988–993.
(20) Phani, A. R.; Passacantando, M.; Santucci, A. *J. Phys. Chem. Solids* **2007**, *68*, 317–323.
(21) (a) Keyson, D.; Volanti, D. P.; Cavalcante, L. S.; Simões, A. Z.; Varela, J. A.; Longo., E. *Mater. Res. Bull.* **2008**, *43*, 771–775. (b) Godinho, M.; Ribeiro, C.; Longo, E.; Leite, E. R. *Cryst. Growth Des.* **2008**, *8*, 384–386.
(22) (a) Schroder, D. K. *Semiconductor Mat. Devise Char.*; John-Wiley: New York, 1990. (b) Longo, V. M.; Cavalcante, L. S.; Erlo, R.; Mastelaro, V. R.; de Figueiredo, A. T.; Sambrano, J. R.; de Lázaro, S.; Freitas, A. Z.; Gomes, L.; Vieira, N. D., Jr.; Varela, J. A.; Longo, E. *Acta Mater.* **2008**, *56*, 2191–2202.
(23) Richard, I. Walton. *Chem. Soc. Rev.* **2002**, *31*, 230–238.
(24) Volanti, D. P.; Cavalcante, L. S.; Keyson, D.; Lima, R. C.; de Moura, A. P.; Moreira, M. L.; Macario, L. R.; Godinho, M. *Met. Mater.* **2007**, *63*, 351.
(25) Rietveld, H. M. *J. Appl. Crystallogr.* **1969**, *2*, 65–71.

(26) Larson, A. C.; Von Dreele, R. B. Los Alamos National Laboratory Report No. LAUR 86-748, 2004.
(27) Finger, L. W.; Cox, D. E.; Jephcoat, A. P. *J. Appl. Crystallogr.* **1994**, *27*, 892–900.
(28) Moreira, M. L.; Pianaro, S. A.; Andrade, A. V. C.; Zara, A. *Mater. Charact.* **2006**, *57*, 193–198.
(29) Edwin, A.; Schauble, J.; Ghosh, P.; Eiler, J. M. *Geochim. Cosmochim. Acta* **2006**, *70*, 2510–2529.
(30) (a) Phillippi, C. M.; Mazdiyasni, K. S. *J. Am. Ceram. Soc.* **1971**, *54*, 254–258. (b) Feinberg, A.; Perry, C. H. *J. Phys. Chem. Solids* **1981**, *42*, 513–518. (c) Perry, C. H.; Liu, D. W.; Ingel, R. P. *J. Am. Ceram. Soc.* **1985**, *68*, 184–187. (d) Kim, B. K.; Hahn, J. W.; Han, K. R. *J. Mater. Sci. Lett.* **1997**, *16*, 669–671. (e) Ishigame, M.; Sakurai, T. *J. Am. Ceram. Soc.* **1977**, *60*, 367–369.
(31) Zyuzin, D. A.; Svetlana, V. C.; Moroz, E. M.; Burgina, E. B.; Sadykov, V. A.; Kostrovskii, V. G.; Matyshak, V. A. *J. Solid State Chem.* **2006**, *179*, 2965–2971.
(32) Xie, S.; Iglesia, E.; Bell, A. T. *Chem. Mater.* **2000**, *12*, 2442–2447.
(33) Dobal, P. S.; Dixit, A.; Katiyara, R. S.; Yu, Z.; Guo, R.; Bhalla, A. S. *J. Appl. Phys.* **2001**, *89*, 8085–8091.
(34) Lee, S. K.; Park, T. J.; Choi, G. *J. Mater. Chem. Phys.* **2003**, *82*, 742–749.
(35) Rabeneau, A. *Angew. Chem., Int. Ed. Engl.* **1985**, *24*, 1026–1040.
(36) (a) Moreira, M. L.; Mambrini, G. P.; Volanti, D. P.; Leite, E. R.; Orlandi, M. O.; Pizani, P. S.; Mastelaro, V. R.; Paiva-Santos, C. O.; Longo, E.; Varela, J. A. *Chem. Mater.* **2008**, *20* (16), 5381–5387. (b) Wilson, G. J.; Matijasevich, A. S.; Mitchell, D. R. G.; Schulz, J. C.; Will, G. D. *Langmuir.* **2006**, *22*, 2016–2027.
(37) Khollam, Y. B.; Deshpande, A. S.; Patil, A. J.; Potdar, H. S.; Deshpande, S. B.; Date, S. K. *Mater. Chem. Phys.* **2001**, *71*, 304–308.
(38) Billinge, S. L. J.; Levin, I. *Science* **2007**, *316*, 516–519.
(39) Wang, Z. L. *J. Phys. Chem. B.* **2000**, *104*, 1153–1175.
(40) Meng, J.; Huang, Y.; Zhang, W.; Du, Z.; Zhu, Z.; Zou, G. *Phys Lett A* **1995**, *205*, 72–76.
(41) (a) Leite, E. R.; Pontes, F. M.; Lee, E. J. H.; Aguiar, R.; Longo, E.; Pontes, D. S. L.; Nunes, M. S. J.; Pizani, P. S., Jr.; Boschi, T. M.; Varela, J. A.; Paskocimas, C. A.; Pinheiro, C. D.; Taft, C. A. *J. Mol. Struct. (Theochem).* **2004**, *668*, 87–91. (b) Longo, V. M.; Cavalcante, L. S.; de Figueiredo, A. T.; Santos, L. P. S.; Longo, E.; Varela, J. A.; Sambrano, J. R.; Parkocimas, C. A.; De Vicente, F. S.; Hernades, A. C. *Appl. Phys. Lett.* **2007**, *90* (091906), 1–3. (c) Paris, E. C.; Espinosa, J. W. M.; de Lazaro, S.; Lima, R. C.; Joya, M. R.; Pizani, P. S.; Leite, E. R.; Souza, A. G.; Varela, J. A.; Longo, E. *Chem. Phys.* **2007**, *335*, 7–14.
(42) Anicete-Santos, M.; Cavalcante, L. S.; Orhan, E.; Paris, E. C.; Simoes, L. G. P.; Joya, M. R.; Rosa, I. L. V.; de Lucena, P. R.; Santos, M. R. M. C.; Santos-Junior, L. S.; Pizani, P. S.; Leite, E. R.; Varela, J. A.; Longo, E. *Chem. Phys.* **2005**, *316*, 260–266.
(43) Wood, D. L.; Tauc, *J. Phys. Rev. B Solid State* **1972**, *5*, 3144–3151.

CG800433H